Electronic Supplementary Material (ESI) for ChemComm.
This journal is © The Royal Society of Chemistry 2019

Supplementary Information

Efficient visible-light driven N_2 fixation over two-dimensional Sb/TiO_2 composites

Zhenqing Zhao,[a] Song Hong,[a] Chao Yan,*[b] Changhyeok Choi,[c] Yousung Jung,*[c] Yongchao Liu,[b] Shizhen Liu,[a] Xin Li,[a] Jieshan Qiu,[a] and Zhenyu Sun*[ad]

[a] State Key Laboratory of Organic-Inorganic Composites, Beijing University of Chemical Technology, Beijing 100029, P.R. China. E-mail: sunzy@mail.buct.edu.cn

[b] Jiangsu University of Science and Technology, School of Material Science and Engineering, Zhenjiang 212003, P. R. China

[c] Graduate School of EEWS, Korea Advanced Institute of Science and Technology (KAIST), Daejeon 34141, Republic of Korea. E-mail: ysjn@kaist.ac.kr

[d] Beijing Key Laboratory of Energy Environmental Catalysis, Beijing University of Chemical Technology, Beijing 100029, P. R. China

Experimental

Materials

Bulk antimony was purchased from Nanjing MKNANO Tech. Co., Ltd. (www.mukenano.com). Isopropanol (IPA), tetra-*n*-butyl titanate ($C_{16}H_{36}O_4Ti$), and ethanol were purchased from Aldrich. NaClO was obtained from Macklin. All chemicals were of analytical grade and used without further purification.

Synthesis of two-dimensional (2D) antimony (Sb nanosheets)

Bulk antimony was ground into powder in a mortar and was dispersed in 400 mL of IPA under bath ultrasonication for 8 h at room temperature. The suspension was then centrifuged at 500 rpm for 5 min. The top two-thirds of the dispersion was pipetted out and subsequently filtered and dried at 60 °C overnight. The obtained Sb nanosheet powder was referred to as Sb.

Synthesis of 2D Sb/TiO_2-x hybrid photocatalysts

Typically, Sb nanosheets (10 mg) and tetra-*n*-butyl titanate (21.27 mg) were dispersed in anhydrous ethanol solution (20 mL) by ultrasound irradiation for 30 min. 5.0 mL of ethanol solution containing 0.5 mL deionized water was added drop-wise into the above dispersion and subjected to ultrasound for 30 min. Subsequently, the mixture was transferred into a petri-dish, and dried at 60 °C. Sb/TiO_2 samples with

different composition ratios were prepared by altering Sb nanosheets/tetra-*n*-butyl titanate weight ratios of 1:0.5, 1:1, and 1:2, and were marked as Sb/TiO_2-1, Sb/TiO_2-2, and Sb/TiO_2-3.

Synthesis of amorphous TiO_2 (a-TiO_2)

Amorphous TiO_2 (a-TiO_2) was synthesized using a similar method as the one applied for the synthesis of Sb/TiO_2 hybrids without adding Sb nanosheets.

Characterization

Powder X-ray diffraction (XRD) measurements were performed with Cu Kα radiation with a D/MAX-RC diffractometer operated at 30 kV and 100 mA, and a 2θ scan rate of 5° min^{-1}. Diffraction patterns were taken over the 2θ range of 20–80°. Raman spectra were collected with a Renishaw in Via Raman microscope with a He/Ne Laser excitation at 532 nm (2.33 eV). X-ray photoelectron spectroscopy (XPS) and VB XPS experiments were performed using Thermo Scientific ESCALAB 250Xi instrument with an electron flood and scanning ion gun. The C 1s binding energy at 284.8 eV was used to correct the charge effects. The UV-vis diffuse-reflectance spectra (DRS) were measured using Persee UV–vis spectroscopy (TU-1950) recorded over a 200–800 nm range, with $BaSO_4$ as the background. The photoluminescence (PL) spectra were acquired on Hitachi F-7000 fluorescence spectrophometer with an excitation wavelength of 349 nm. TEM (HAADF-STEM) was conducted using a JEOL ARM200 microscope with 200 kV accelerating voltage. TEM samples were prepared by depositing a droplet of sample suspension in ethanol onto a Cu grid coated with a lacey carbon film. EPR spectra were obtained using a Bruker e-scan EPR spectrometer (27 °C, 9.7397 GHz).

Electrochemical measurements

The electrochemical analysis was performed via a CHI 660D electrochemical workstation (Shanghai Chenhua, China) using a standard three-electrode quartz cell. A Xe lamp (MerryChange MC-X301) was used as a light source. To make a working electrode, catalyst powder was deposited on an indium tin oxide (ITO) substrate by Nafion coating. In brief, 1.2 mg of a catalyst was suspended in 200 μL of IPA/H_2O solution (volume ratio of 1:1) and 1 μL of 5% Nafion solution, and the mixture was ultrasonically dispersed for 60 min. Then, the obtained slurry was coated onto the ITO glass. After evaporation of IPA, the catalyst-coated ITO substrate was used as a working electrode. During electrochemical impedance measurements and photocurrent tests, the electrolyte of 0.5 M Na_2SO_4 solution was bubbled with Ar.

Photocatalytic test

Photocatalytic N_2 fixation was carried out in a cylindrical stainless-steel reactor with a quartz window (diameter = 2.5 cm) on the top. In a typical photocatalytic test, 5 mL of aqueous solution containing 20% methanol (photogenerated hole scavenger) was added into the reactor and charged with N_2 to 0.3 MPa after removal of air under vacuum for three times. The reactor was then sealed and irradiated under visible light irradiation (Xenon lamp with a cut off filter, $\lambda \geq 420$ nm). The gas was bubbled into a tail gas absorber containing 10 mL of 0.1 M HCl solution, and the solution was tested in the same method. The liquid products were centrifuged to remove the catalyst and tested by the indophenol blue method.

To test the catalyst reusability, used catalyst was recovered by centrifugation after reaction, and washed with distilled water for at least 3 times and dried at 60 °C overnight for the next run.

Determination of ammonia

NH_4^+ concentration analysis was conducted using the indophenol blue method. In brief, 2.0 mL of product solution was transferred to a 5 mL bottle. Then, 2 mL of 1 M NaOH solution containing 5 w% salicylic acid and 5 w% sodium citrate was added, followed by adding 1 mL of 0.05 M NaClO aqueous solution and 0.2 mL of 1 w% $Na[Fe(NO)(CN)_5]$ aqueous solution and homogeneously mixed. The absorption spectrum was carried out using a UV-vis spectrophotometer after standing for 2 h at room temperature. The absorbance at the wavelength of 655 nm was used to determine the concentration. Absolute calibrations of this method including methanol system and HCl system were conducted using standard ammonium chloride solutions (Figs. S6 and S7).

Calculation of the NH_3 yield rate and the turnover frequency per surface site (TOF)

The NH_3 yield rate can be estimated using the following equation:

$$NH_3 \text{ yield rate} = (c_{NH3} \times V)/(t \times m) \quad \text{Eq. S1}$$

where $c_{NH3}$is the measured NH_3 concentration, V is the volume of the aqueous solution (5 mL), t is reaction time, and m is the total mass of the catalyst. The NH_3 yield rate and corresponding error bars reported in this work were obtained based on the measurements of at least two separately prepared samples under the same conditions.

The turnover frequency per surface site can be estimated using the following equation:

$$TOF = \frac{the\ moles\ of\ evoled\ NH_3}{the\ moles\ of\ cocatalyst\ on\ photocatalyst\ \times\ reaction\ time} \quad \text{Eq. S2}$$

The as-obtained Sb/TiO_2-1 exhibited a TOF of about 0.19 h^{-1}, outperforming many other photocatalytic N_2 conversion catalysts (see Table S1).

Computational details

Structure relaxation and total electronic energy calculations were performed using spin-polarized density functional theory (DFT) methods implemented in the Vienna ab initio simulation package (VASP).[1-4] We used PBE functional with Grimme's D3 dispersion correction and Becke-Johnson (BJ) damping.[5-7] A cut-off energy for plane wave basis set was set to 400 eV. Structure relaxations were performed until the energy differences and residual forces of each atom become less than 10^{-5} eV and 0.05 eV / Å, respectively.

We used (110) surface of rutile TiO_2 for modelling amorphous TiO_2. The (2x1) surface supercell with four TiO_2 layers was considered. For Sb, (2x2) atomic supercell of (001) surface with six atomic layer was used. The k-points were sampled with using (4 x 4 x 1) and (3 x 3 x 1) Monkhorst-Pack mesh for TiO_2 (110) and Sb (001), respectively.[8] All slab models include enough vacuum (> 18 Å) along c-axis. Only the adsorbates and top most two layers were allowed to relax, while other layers were fixed to their optimized bulk positions.

The computational hydrogen electrode (CHE) model developed by Nørskov and co-workers was employed to establish free energy diagram for electrochemical reaction.[9] The calculated thermal energies for gas molecules and adsorbents to convert electronic energies into Gibbs free energies are listed in Table S2. The required free energy for the largest free energy requiring reaction intermediate step (or PDS, potential determining step) is 0.75 eV on O-vacancy site in TiO_2 ($*N_2 + (H^+ + e^-) \rightarrow *NNH$), which is significantly lower than that of Sb(001), 2.25 eV ($*N_2 + (H^+ + e^-) \rightarrow *NNH$). Based on these DFT calculations, we suggest that the O-vacancy sites in TiO_2 seem to be the main catalytic sites that can promote N_2 reduction in Sb/TiO_2 and the role of Sb is mainly to increase the number of photoexcited electrons transferred to TiO_2 which, otherwise, has a large band-gap energy of 3.64 eV hindering generation of sufficient amounts of photoexcited electrons.

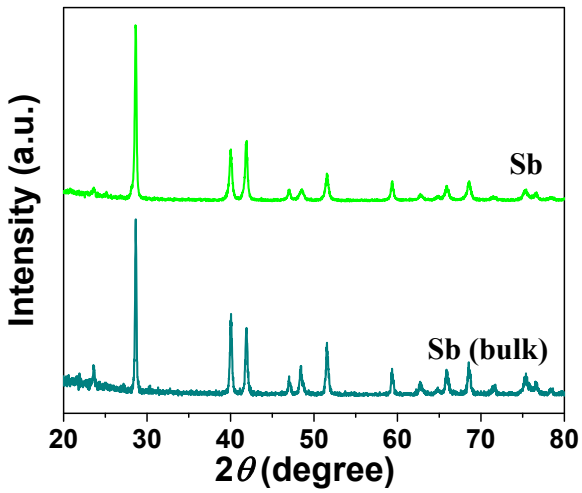

Fig. S1 The XRD patterns of Sb (bulk) and Sb.

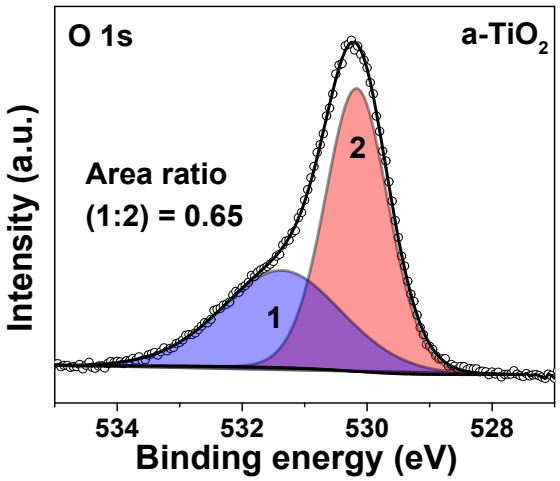

Fig. S2 The O 1s XPS spectrum of a-TiO_2.

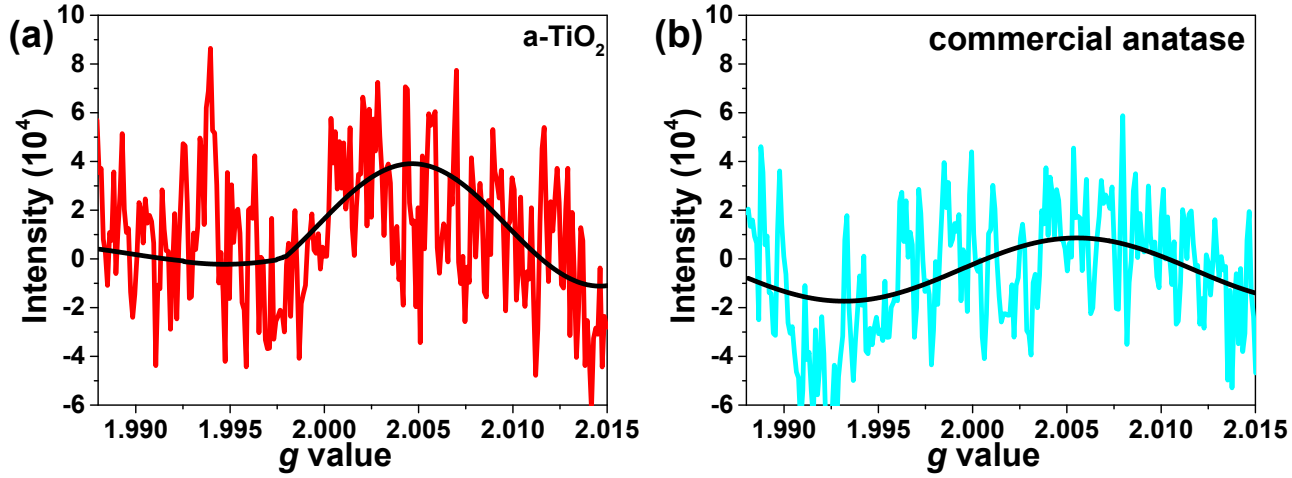

Fig. S3 EPR spectra of (a) a-TiO_2 and (b) commercial anatase.

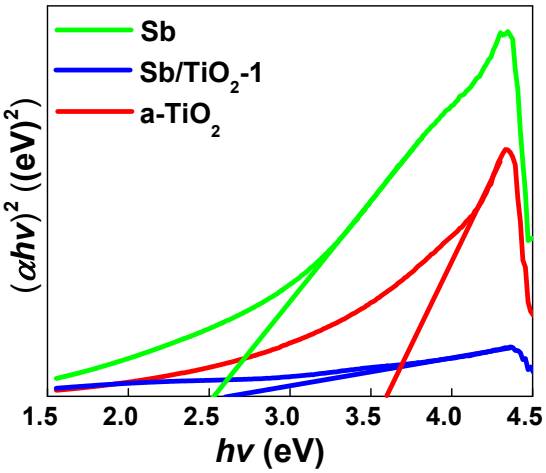

Fig. S4 Tauc plots of a-TiO_2, Sb nanosheets, and Sb/TiO_2-1.

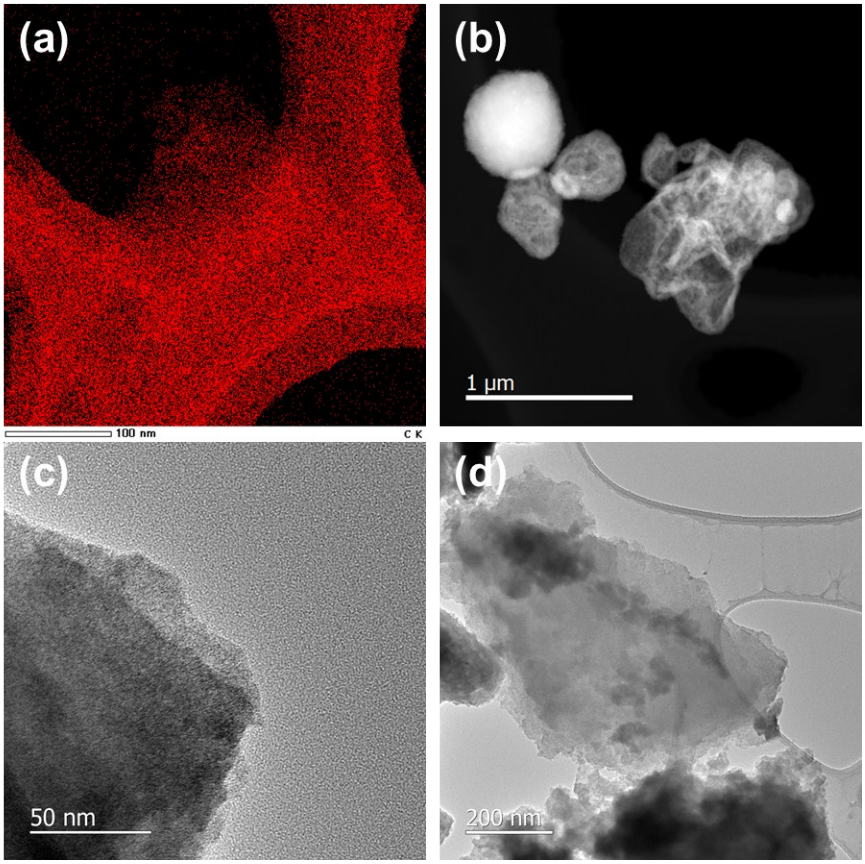

Fig. S5 (a) EDX map of C element. (b, c, and d) Low-magnification TEM images of Sb/TiO_2-1.

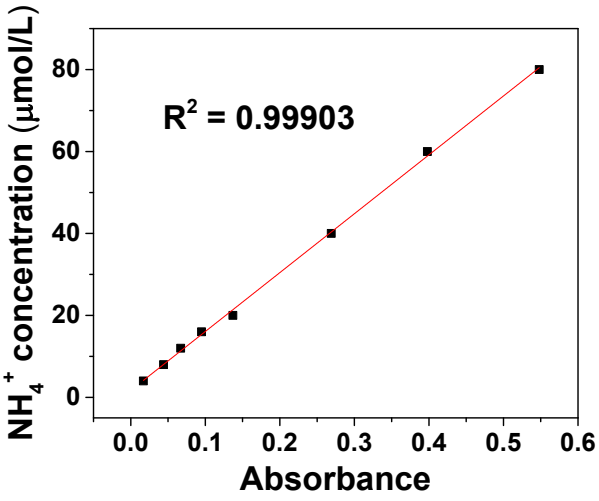

Fig. S6 Absolute calibrations in methanol system using standard ammonium chloride solutions.

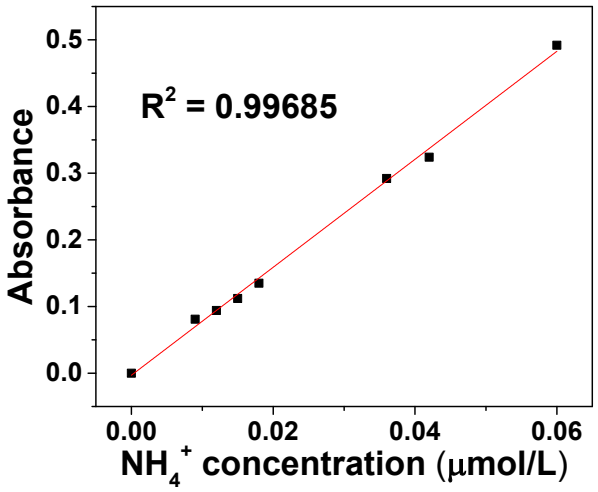

Fig. S7 Absolute calibrations in HCl system using standard ammonium chloride solutions.

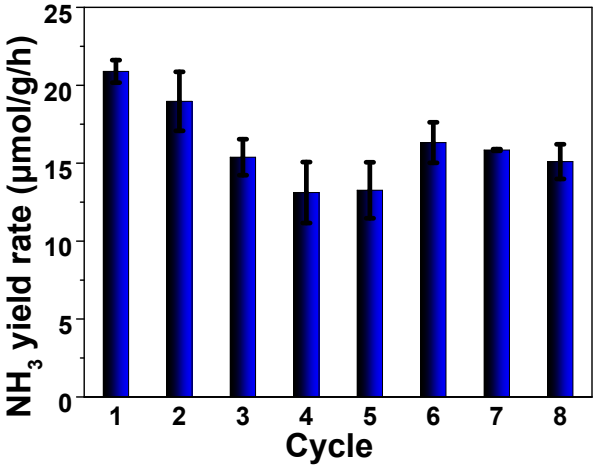

Fig. S8 NH_3 yield rate of Sb/TiO_2-1 versus recycle times.

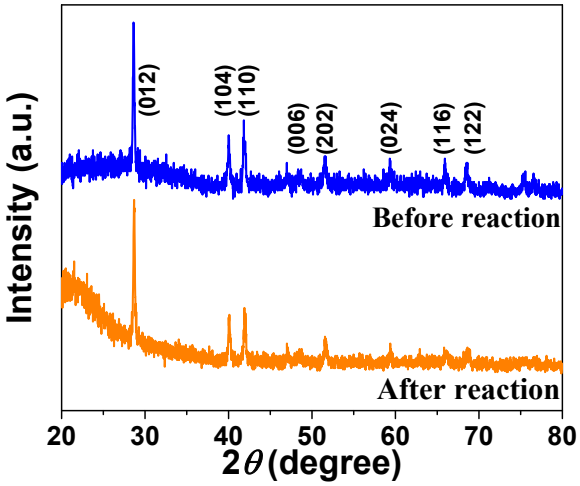

Fig. S9 The XRD patterns of Sb/TiO_2-1 before and after the N_2 photoreduction reaction.

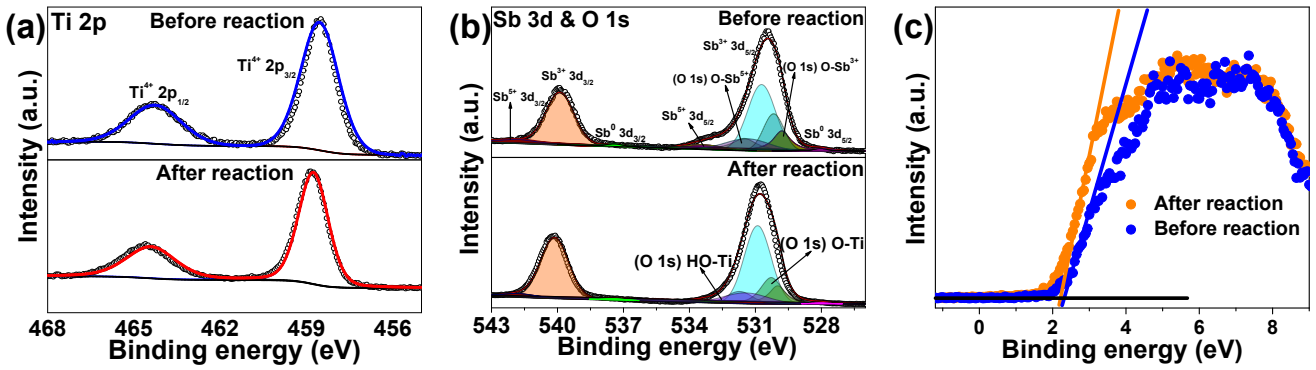

Fig. S10 (a) Ti 2p, (b) deconvoluted Sb 3d and O 1s, and (c) valence-band XPS spectra of Sb/TiO_2-1 before and after the N_2 photoreduction reaction.

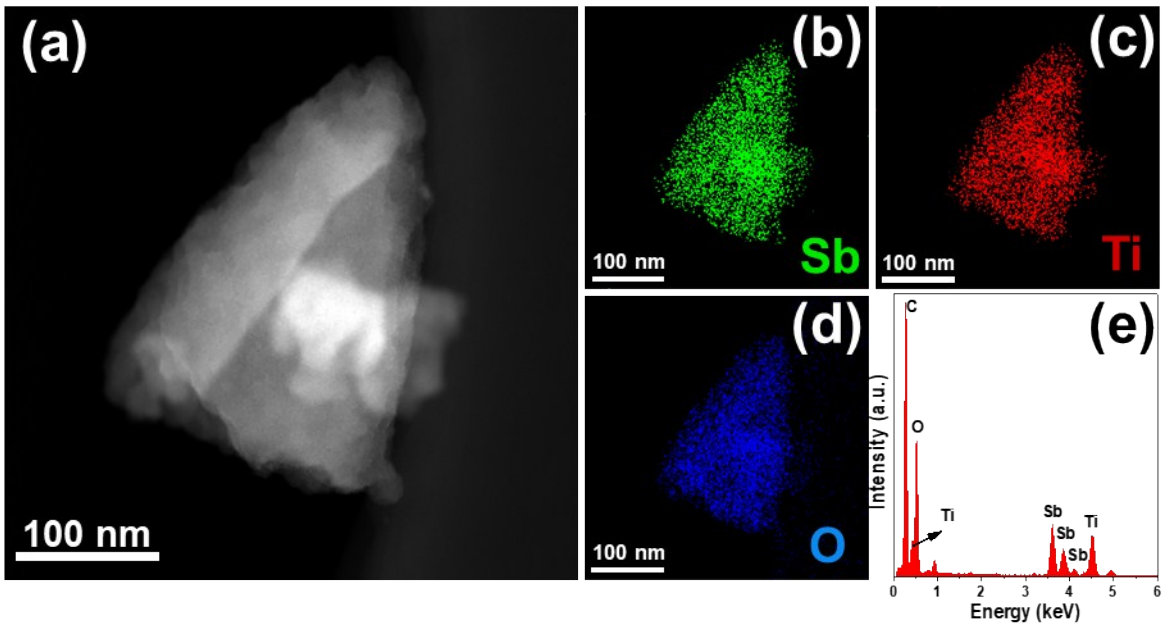

Fig. S11 (a) HAADF-STEM image of Sb/TiO_2-1 after N_2 photoreduction reaction and corresponding EDX maps of (b) Sb, (c) Ti, (d) O elements, and (e) EDX spectrum.

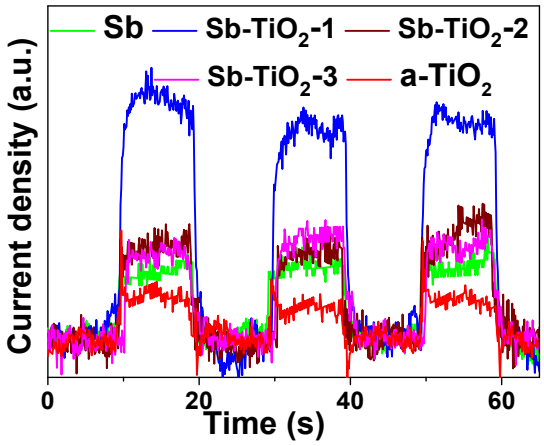

Fig. S12 Photocurrent responses of Sb nanosheets, a-TiO_2, and Sb/TiO_2-x recorded in Ar atmosphere.

Table S1. Comparison of N_2 photoreduction performance among reported catalysts.

Catalyst	Light source	Reaction medium	Temperature	NH_3 yield rate ($\mu mol\ g^{-1}\ h^{-1}$)	TOF (h^{-1})	Ref.
Sb/TiO_2-1	300 W Xenon lamp with a 420 nm cut off filter	Methanol (20 vol%) aqueous solution	Room Temperature	20.8	0.19	This work
Ru-TiO_2	300 W Xenon lamp	Ethanol (20 vol%) aqueous solution	Room temperature	3.31	/	[10]
Ru/TiO_2	150 W Xenon lamp	Methanol (5 vol%) aqueous solution	N/A	17.3	/	[11]
Rh/TiO_2	150 W Xenon lamp	Methanol (5 vol%) aqueous solution	N/A	12.6	/	[11]
Pd/TiO_2	150 W Xenon lamp	Methanol (5 vol%) aqueous solution	N/A	11.8	/	[11]
Pt/TiO_2	150 W Xenon lamp	Methanol (5 vol%) aqueous solution	N/A	4.8	/	[11]
Fe/3D Graphene	500 W Hg Lamp	Gaseous H_2/N_2 v/v 3:1, 20 mL min^{-1}	200 °C	24	/	[12]
MoS_2	500 W Xe lamp with a 420 nm cut off filter	Water	25 °C	325	0.011	[13]
Fe_2O_3	500 W Xe lamp	789 mg L^{-1} ethanol aqueous solution	25 °C	90	0.014	[14]
BiOBr	300 W Xe lamp with a 420 nm cut off filter	Water	25 °C	102	0.031	[15]
N−TiO_2	300 W Xe lamp	150 mL of deionized water, and 0.12 g of ethanol aqueous solution	N/A	667.5	0.11	[16]
Fe−TiO_2	300 W Xe lamp	150 mL of deionized water, and 0.12 g of ethanol aqueous solution	N/A	824.55	0.13	[16]
V−TiO_2	300 W Xe lamp	150 mL of deionized water, and 0.12 g of ethanol aqueous solution	N/A	876.6	0.14	[16]
Fe−N−TiO_2	300 W Xe lamp	150 mL of deionized water, and 0.12 g of ethanol aqueous solution	N/A	985.58	0.16	[16]
Fe−V−TiO_2	300 W Xe lamp	150 mL of deionized water, and 0.12 g of ethanol aqueous solution	N/A	1108.72	0.18	[16]
JRC-TIO-6	300 W Hg Lamp	0.1 M KPi solutions	Ambient temperature	0.73	0.0105	[17]
$Mo_2Fe_6S_8$–Sn_2S	150 W Xenon lamp, 100 mW cm^{-2}	5 mM ascorbic acid, 50 mM pyridinium hydrochloride in 10 mL aqueous solution	Ambient temperature	/	0.111	[18]
FeMoS–FeS–SnS chalcogel	150 W Xenon lamp, 100 mW cm^{-2}	5 mM ascorbic acid, 50 mM pyridinium hydrochloride in 10 mL aqueous solution	Ambient temperature	/	0.177	[19]

Table S2. Calculated thermal energies for gas molecules and adsorbates on TiO_2 (110) in eV.

Species	ZPE	$\int C_p\,dT$	-TS
H_2	0.27	0.09	-0.40
N_2	0.14	0.09	-0.59
NH_3	0.85	-0.10	-0.60
$*N_2$	0.19	0.09	-0.20
*NNH	0.50	0.07	-0.12
$*NNH_2$	0.86	0.06	-0.10
*NHNH	0.83	0.06	-0.09
$*NHNH_2$	1.18	0.07	-0.11
$*NH_2NH_2$	1.49	0.11	-0.24
*N	0.08	0.03	-0.04
*NH	0.34	0.05	-0.07
$*NH_2$	0.71	0.04	-0.07
$*NH_3$	1.02	0.07	-0.14

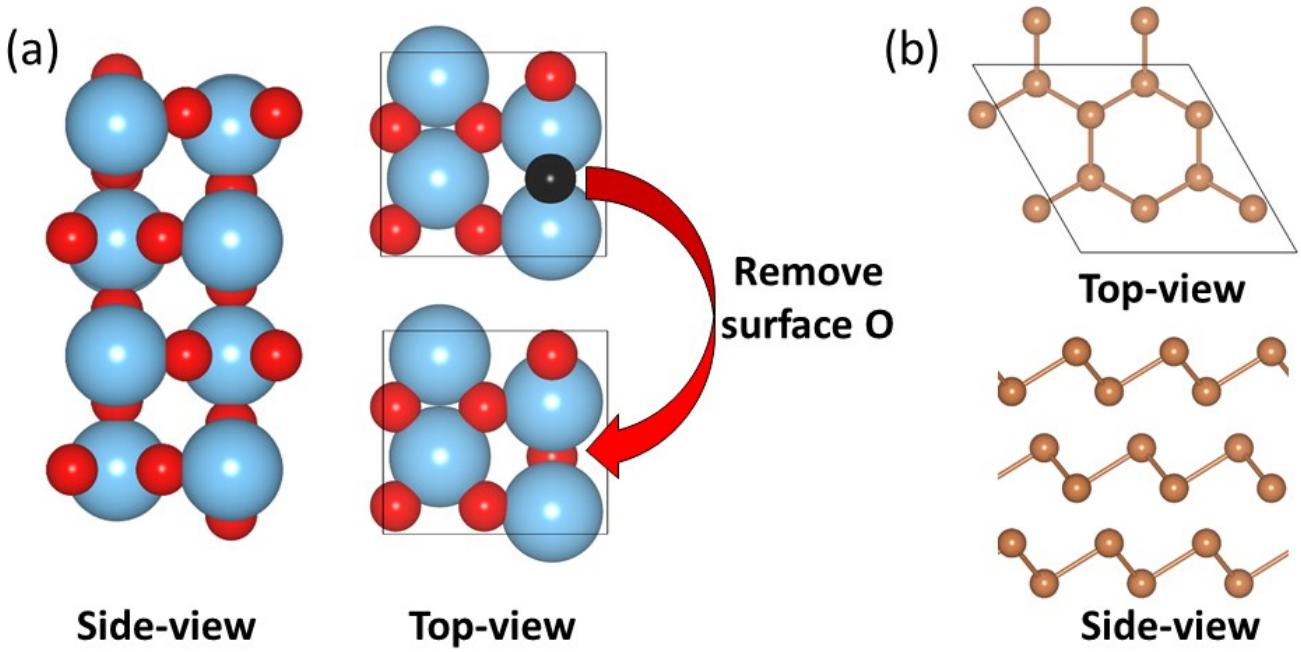

Fig. S13 Calculation models of (a) O-vacancy containing rutile-TiO_2(110) and (b) Sb(001). Sky blue, red and orange balls represent Ti, O and Sb atoms, respectively. Black ball in (a) indicates removed surface O in TiO_2 to construct O-vacancy. In top-view, only topmost layer is shown for the clarity.

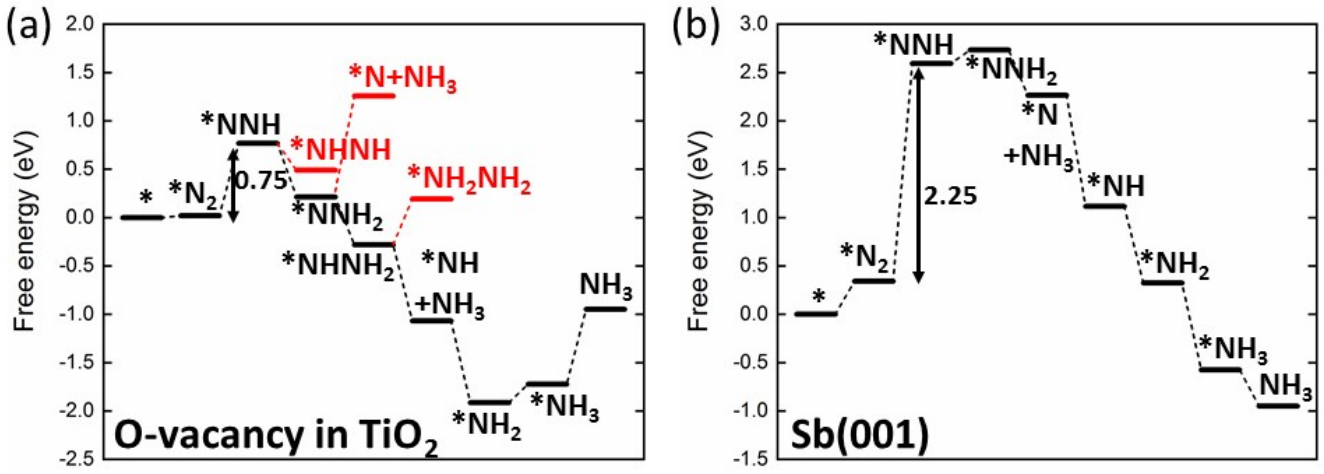

Fig. S14 Free energy diagram of N_2 reduction on (a) O-vacancy containing rutile-TiO_2(110) and (b) Sb(001). Black line indicates the lowest energy requiring energy pathway, while red line indicates less favourable pathway. The free energy at the largest free energy requiring reaction step is shown.

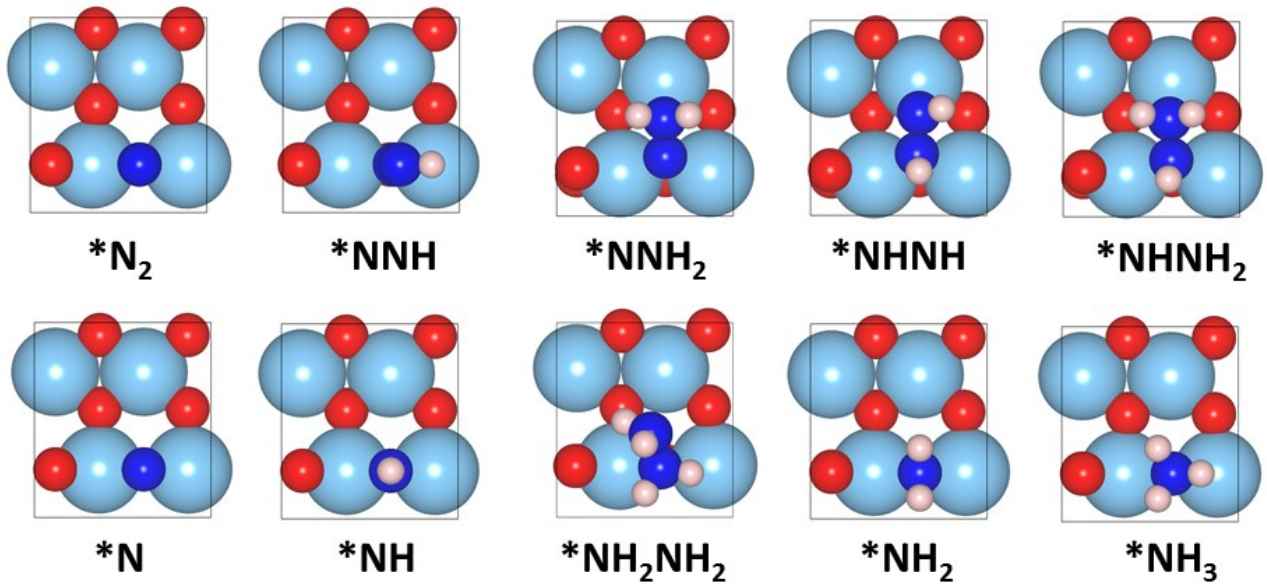

Fig. S15 The optimized geometries of reaction intermediates for N_2 reduction on O-vacancy containing rutile-TiO_2 (110). Sky blue, red, blue and ivory balls represent Ti, O, N and H atoms, respectively. Only the topmost layer and adsorbents were shown for the clarity.

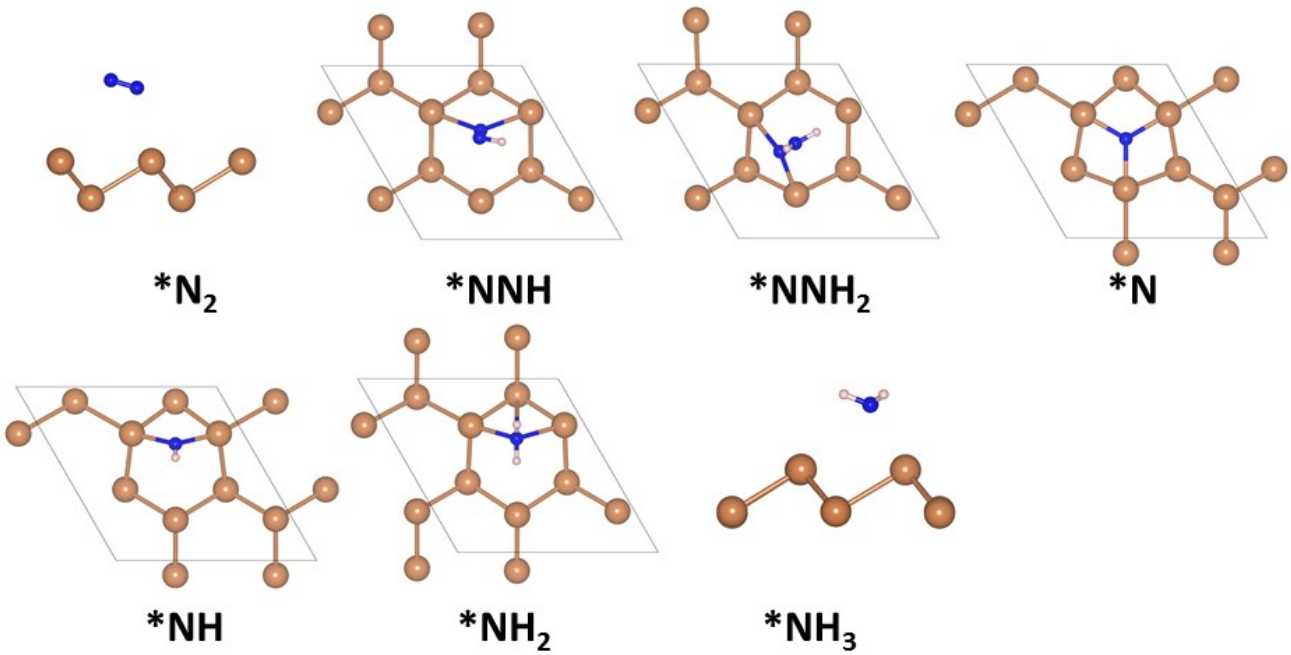

Fig. S16 The optimized geometries of reaction intermediates for N_2 reduction on Sb(001). Orange, blue and ivory balls represent Sb, N, and H atoms, respectively. Only the topmost layer and adsorbents were shown for the clarity.

References

1. P. E. Blöchl, *Phys. Rev. B*, 1994, **50**, 17953-17979.
2. G. Kresse and J. Furthmüller, *Phys. Rev. B*, 1996, **54**, 11169.
3. G. Kresse and J. Furthmüller, *Comput. Mater. Sci.*, 1996, **6**, 15-50.
4. G. Kresse and D. Joubert, *Phys. Rev. B*, 1999, **59**, 1758.
5. J. P. Perdew, K. Burke and M. Ernzerhof, *Phys. Rev. Lett.*, 1996, **77**, 3865.
6. S. Grimme, J. Antony, S. Ehrlich and H. Krieg, *J. Chem. Phys.*, 2010, **132**, 154104.
7. S. Grimme, S. Ehrlich and L. Goerigk, *J. Comput. Chem.*, 2011, **32**, 1456-1465.
8. H. J. Monkhorst and J. D. Pack, *Phys. Rev. B*, 1976, **13**, 5188.
9. J. K. Nørskov, J. Rossmeisl, A. Logadottir, L. Lindqvist, J. R. Kitchin, T. Bligaard and H. Jonsson, *J. Phys. Chem. B*, 2004, **108**, 17886-17892.
10. S. Liu, Y. Wang, S. Wang, M. You, Z. Zhao, G. Jiang, J. Qiu, B. Wang and Z. Sun, *ACS Sustainable Chem. Eng.*, 2019, **7**, 6813–6820.
11. K. T. Ranjit, T. K. Varadarajan and B. Viswanathan, *J. Photochem. Photobiol. A*, 1996, **96**, 181–185.
12. Y. Lu, Y. Yang, T. Zhang, Z. Ge, H. Chang, P. Xiao, Y. Xie, L. Hua, Q. Li, H. Li, B. Ma, N. Guan, Y. Ma and Y. Chen, *ACS Nano*, 2016, **10**, 10507-10515.
13. S. Sun, X. Li, W. Wang, L. Zhang and X. Sun, *Appl. Catal. B*, 2017, **200**, 323-329.
14. M. Lashgari and P. Zeinalkhani, *Appl. Catal. A*, 2017, **529**, 91-97.
15. H. Li, J. Shang, Z. Ai and L. Zhang, *J. Am. Chem. Soc.*, 2015, **137**, 6393-6401.
16. C. Tian, W. Sheng, H. Tan, H. Jiang and C. Xiong, *ACS Appl. Mater. Interfaces*, 2018, **10**, 37453-37460.
17. H. Hirakawa, M. Hashimoto, Y. Shiraishi and T. Hirai, *J. Am. Chem. Soc.*, 2017, **139**, 10929-10936.
18. A. Banerjee, B. D. Yuhas, E. A. Margulies, Y. Zhang, Y. Shim, M. R. Wasielewski and M. G. Kanatzidis, *J. Am. Chem. Soc.*, 2015, **137**, 2030-2034.
19. J. Liu, M. S. Kelley, W. Wu, A. Banerjee, A. P. Douvalis, J. Wu, Y. Zhang, G. C. Schatz and M. G. Kanatzidis, *J. Photochem. Photobiol. A*, 2016, **113**, 5530.